OPEN ACCESS

Coherent x-ray production via pulse reflection from laser-driven dense electron sheets

New Journal of Physics
The open-access journal for physics

Coherent x-ray production via pulse reflection from laser-driven dense electron sheets

B Qiao[1,2,3], M Zepf[1], M Borghesi[1], B Dromey[1] and M Geissler[1]

[1] Centre for Plasma Physics, School of Mathematics and Physics, Queen's University Belfast, Belfast BT7 1NN, UK
[2] Institute for Advanced Simulation, Forschungzentrum Jülich GmbH, D-52425, Jülich, Germany
E-mail: b.qiao@qub.ac.uk

New Journal of Physics **11** (2009) 103042 (11pp)
Received 17 July 2009
Published 26 October 2009
Online at http://www.njp.org/
doi:10.1088/1367-2630/11/10/103042

Abstract. A scheme to obtain brilliant x-ray sources by coherent reflection of a counter-propagating pulse from laser-driven dense electron sheets is theoretically and numerically investigated in a self-consistent manner. A radiation pressure acceleration model for the dynamics of the electron sheets blown out from laser-irradiated ultrathin foils is developed and verified by PIC simulations. The first multidimensional and integral demonstration of the scheme by 2D PIC simulations is presented. It is found that the reflected pulse undergoes Doppler-upshift by a factor $4\gamma_z^2$, where $\gamma_z = (1 - v_z^2/c^2)^{-1/2}$ is the effective Lorentz factor of the electron sheet along its normal direction. Meanwhile the pulse electric field is intensified by a factor depending on the electron density of the sheet in its moving frame n_e/γ, where γ is the full Lorentz factor.

[3] Author to whom any correspondence should be addressed.

Contents

1. Introduction

The quest for high-quality x-ray sources has been pursued for many years since the emergence of optical lasers [1]. Coherent, brilliant x-ray sources have broad applications from imaging complex molecules to medical diagnostics due to the short wavelengths and high photon energies. Several techniques have been under investigation, including plasma-based x-ray lasers [2], free-electron lasers [3] and high-order harmonics generated in gases by ultrafast lasers [4].

Another route towards brilliant x-ray sources is Thomson scattering of laser photons with frequency ω_i from relativistic electrons with energies γmc^2. The scattering upshifts photon frequency to $\omega_r = \gamma^2(1-\beta\cos\theta)^2\omega_i$ due to relativistic Doppler effect, where $\beta = v/c$ is the electron velocity normalized to the light speed c and θ is the scattering angle. However, usually the density of relativistic electrons either from conventional accelerators or from laser-driven electron beams [5] is rather low and so the scattered x-ray pulse is incoherent. Conversely, coherent Thomson scattering should be obtained from electron sheets with sufficiently high density such that a large number N of electrons resides in a volume λ_R^3, where λ_R is laser wavelength in the rest frame of the sheet. Such dense electron sheet, moving close to velocity of c, can coherently reflect laser pulses like a '*relativistic mirror*'.

Relativistic mirrors can be created in the form of diverging electron density spikes of the wake wave by laser pulses propagating through underdense plasmas [6]. Scattering signal with $\gamma \approx 5$ from the spike has been measured experimentally [7]. However, coherent scattering with higher γ values is difficult, as this leads to a decrease in the electron density of the mirror. Alternatively, relativistic mirrors can also be obtained when irradiating solid targets with intense linearly polarized laser pulses. The light pressure drives electron oscillations near the critical plasma surface, leading to an oscillating mirror and high harmonic generation (HHG) in the reflected pulse [8]. Harmonic orders up to 3200 corresponding to 3.7 keV photons have been measured [9]. However, the spectral bandwidth is very broad due to the ultrashort velocity spike where coherent emission occurs.

Recently, it was found [10] that ultrashort dense electron sheets can be generated from ultrathin foils by intense laser pulses in the blow-out regime. In the blow-out regime, all foil electrons are separated from the ions and synchronously accelerated to relativistic energies forming a dense electron sheet. This sheet has extremely small thickness (a few nanometers),

near-solid density and velocity close to c, so that it can be used as a relativistic electron mirror (REM). Such an extreme optics are suitable for coherent reflection of a second counter-propagating pulse for frequency upshift, pulse compression and amplitude intensification. This opens a novel scheme to obtain coherent, brilliant x-ray sources, realizable with the present-day technology. However, the basic tenet of this novel scheme is still unclear so far. All the current studies [11, 12] treat only separate, single aspects of the problem, and are based on one-dimensional (1D) particle-in-cell (PIC) simulations for very short pulses (few-cycles). To our best knowledge, no self-consistent and complete demonstration of the scheme in a more realistic multidimensional case has yet been presented.

In this paper, we integrally and self-consistently investigate the scheme to obtain brilliant x-ray sources via coherent reflection of a counter-propagating pulse from laser-driven dense electron sheets, applying theoretical modeling and 2D PIC simulations. An analytical radiation pressure acceleration (RPA) model for the dynamics of electron sheets from laser-irradiated ultrathin foils is developed. The frequency upshift and amplitude intensification of the reflected pulse from such electron sheets are quantitatively analyzed. The 2D PIC simulations give the first complete demonstration of the scheme and a quantitative verification of the theory, providing an extremely strong guide to future experiments. The simulation results are presented in detail for two reference cases in movies 1 and 2.

2. Theoretical model

2.1. RPA model for dynamics of dense electron sheets

In order to blow out all foil electrons, the laser ponderomotive force $(\mathbf{v}/c) \times \mathbf{B}_\mathrm{L} \sim E_\mathrm{L}$ has to be larger than the maximum electrostatic field $E_{\mathrm{s,max}} = 4\pi e n_0 l_0$ induced due to the charge separation. This means that the foil thickness l_0 should satisfy

$$\frac{l_0}{\lambda} < \frac{1}{2\pi}\frac{n_\mathrm{c}}{n_0}a_0, \tag{1}$$

where $a_0 = eE_0/mc\omega$ is the normalized amplitude of laser electric field, e and m are electron charge and mass, λ and ω are laser wavelength and frequency, $n_c = m\omega^2/4\pi e^2$ is the critical plasma density, and n_0 is the initial foil density.

In order to analyze the acceleration mechanism of electrons in the blow-out regime, at first we run a 1D PIC simulation. A linearly polarized laser pulse with intensity $I_0 = 5 \times 10^{21}\,\mathrm{W\,cm^{-2}}$ ($a_0 = 60$) and $\lambda = 1\,\mu\mathrm{m}$ is normally incident on a thin foil with thickness $l_0 = 5\,\mathrm{nm}$ and density $n_0 = 200n_\mathrm{c}$ from time $t = 0$. The results are shown in figure 1. Due to the strong radiation pressure, all foil electrons are quickly blown out, forming a dense electron sheet co-moving with the laser pulse (surfing near the pulse front). An electron depletion region is left behind which increases with time. The charge separation electric field E_z is uniform (equals to $4\pi n_0 el/(mc\omega/e) \approx 6.28$) between the electron sheet and the slowly-expanding ions while it steeply decreases within the sheet down to zero at the right surface. Because the sheet is much thinner than the skin depth as $l_0 \ll \lambda_\mathrm{s} \approx c/\omega_\mathrm{p}$, the pulse front is penetrating through the sheet with its electric field exponentially damped due to the energy transfer to electrons, and then each electron is accelerated according to the local laser field. Therefore, a simple RPA model [13]–[15] can be developed to describe the dynamics of the blown-out dense electron sheets. Assuming the foil electron sublayers with different z_r (z_r is the relative position to the left boundary of the foil, $0 \leqslant z_\mathrm{r} \leqslant l_0$) keep their relative orders and are not compressed, the

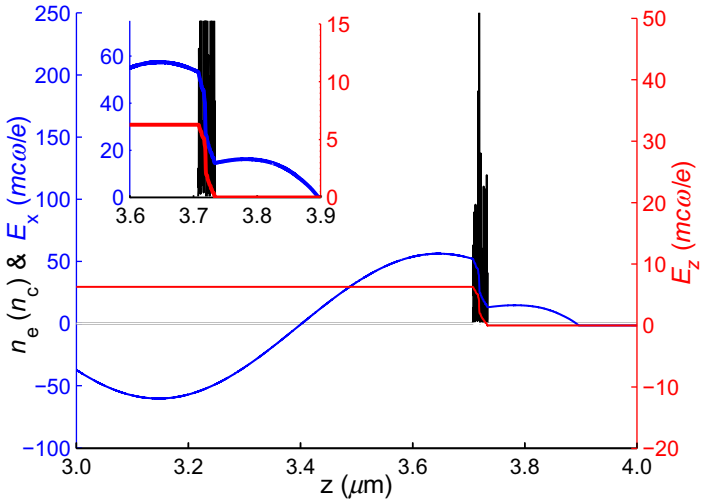

Figure 1. 1D PIC simulation results: electron density n_e/n_c (black), laser field E_x (blue), and charge separation field E_z (red) at $t = 4T$ ($T = 2\pi/\omega$), also zoomed in inset, for foil with initial density $n_0 = 200n_c$ and thickness $l_0 = 5$ nm irradiated by x-polarized laser at amplitude $a_0 = 60$ and wavelength $\lambda = 1\ \mu$m.

motion for electrons initially at $z = z_0 + z_r$ (z_0 is the initial position of the foil left boundary) in the blow-out regime can be described by the equation

$$\frac{dp}{dt} = \frac{E_L^2(t, z)\exp(-2z_r/l_0)}{2\pi n_0 l_0}\frac{\sqrt{m_e c^2 + p^2} - p}{\sqrt{m_e c^2 + p^2} + p} - eE_s(z_r), \tag{2}$$

where the first term represents the radiation pressure of the local laser electric field $E(t, z, z_r)$, which can be described as

$$E(t, z, z_r) \approx E_L(t, z)\exp(-z_r/l_0) \approx E_0\cos(\omega t - kz)\exp(-z_r/l_0), \tag{3}$$

$E_s(z_r)$ is the charge separation electric field, which is approximately defined as

$$E_s \approx 4\pi n_0 e l_0(1 - z_r/l_0). \tag{4}$$

Equations (2)–(4) effectively describe the collective dynamics of dense electron sheet blownout from ultrathin foils by intense laser pulses. This RPA model is completely different from those in previous publications [10, 12], where all the models are restricted to a schematic single-cycle laser pulses and are essentially a single particle model. The 2D PIC simulation results, as discussed later, further indicate that this RPA model is also effective in the multidimensional cases.

The coordinates of electrons initially at the leftmost ($z_r = 0$) and rightmost ($z_r = l_0$) sides of the foil varying with time by equations (2)–(4) are plotted in figure 2, in good agreement with 1D (2(a)) and, as discussed later, 2D (2(b)) PIC simulation results. Due to the nonuniform E_s within the sheet and the oscillating ponderomotive force, we see in figure 2(a) that the acceleration of the leftmost electrons is slower than that of the rightmost, and at $t \approx 12T$ ($T = 2\pi/\omega$) the leftmost electrons turn back and the electron sheet starts to debunch (with density decreasing and thickness widening). Therefore, the dense electron sheet can be considered as a transient

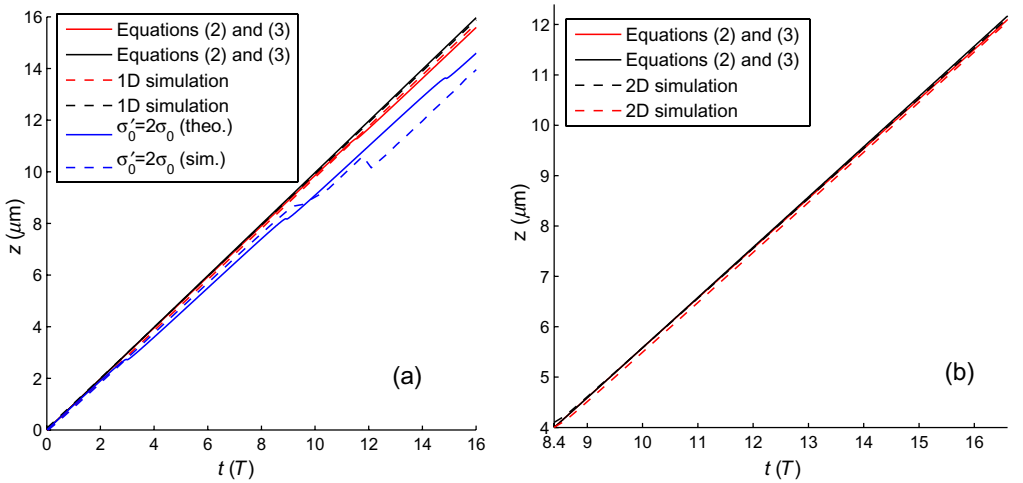

Figure 2. Coordinates of the leftmost ($z_r = 0$) (red lines) and the rightmost ($z_r = l_0$) (black lines) electrons in the electron sheet as function of time t: (a) solid lines are the analytical solutions of equations (2)–(4) with initial condition $t_0 = 0$ and $z_0 = 0$, dashed lines are 1D PIC simulation results of figure 1; (b) solid lines are the analytical solutions of equations (2)–(4) with $t_0 = 8.4T$ and $z_0 = 4.0\,\mu$m, dashed lines are 2D simulation results of the following figure 3. The blue solid/dashed lines in (a) are the results for the leftmost electrons if the initial foil area density is increased to $\sigma_0' = 2\sigma_0 = 2n_0l_0$ (those for the rightmost electrons are close to the black lines, not plotted here).

coherent structure with a limited time duration. We can easily see from equations (2)–(4) that this time duration, defined as the life time of the electron sheet, depends critically on the laser amplitude a_0 and the foil areal density $\sigma_0 = n_0l_0$. Smaller values for a_0 or larger values for σ_0 will decrease the life time, shown by the blue lines in figure 2(a) corresponding to the case with initial foil area density $\sigma_0' = 2\sigma_0$. In the scheme for coherent production of x-ray sources that we discuss, the dense electron sheet acts, within its life time, as a stable relativistic mirror.

2.2. *Quantitative analysis for the reflected pulse*

In the second part, we self-consistently show that this blown-out dense electron sheet can be used as a near-ideal REM to coherently reflect a counter-propagating probe pulse for frequency upshift and amplitude intensification. Choosing the probe pulse to be normally incident on the sheet, the frequency of the reflected pulse will be upshifted as

$$\omega_r = \frac{1+\beta_z}{1-\beta_z}\omega_i \approx 4\gamma_z^2\omega_i, \tag{5}$$

where $\beta_z = v_z/c$ is the normalized velocity and $\gamma_z = (1-\beta_z^2)^{-1/2}$ is the effective Lorentz factor of the REM along its normal direction, ω_i is the frequency of the incident probe pulse. Assuming the probe pulse to be weak enough to have negligible effects on the REM dynamics, only the linear reflectivity is considered. Similarly to the derivations in [6, 12, 18], we start from the

wave equation for the vector potential of the reflected pulse in the REM rest frame

$$\frac{\partial^2}{\partial t^2}A'_{\rm r} - c^2\frac{\partial^2}{\partial z^2}A'_{\rm r} + \frac{4\pi e^2 n_{\rm e}}{m_{\rm e}\gamma}A'_{\rm i} = 0, \tag{6}$$

where $A'_{\rm r}$ and $A'_{\rm i}$ are the vector potentials, respectively, of the reflected and incident probe pulses, $A_{\rm r}$ and $A_{\rm i}$ are those in the lab frame, $\gamma = (1 - v^2/c^2)^{-1/2}$ is the full Lorentz factor of the REM, $n_{\rm e}$ is its electron density and $n'_{\rm e} = n_{\rm e}/\gamma$. Note that $A'_{\rm i} = E'_{\rm i}/\omega'_{\rm i} = E_{\rm i}/\omega_{\rm i} = A_{\rm i}$ due to the conservation of photon numbers.

As analyzed above, the blown-out dense electron sheet within its lifetime is a coherent structure having extremely small thickness at a few nanometers, generally smaller than the wavelength of the reflected pulse. Therefore, the probe pulse experiences a volume reflection from the sheet just like the reflection from an ideal mirror, where the density distribution of the sheet is effectively unimportant. For simplicity, it is reasonable to assume that $n_{\rm e}$ in the REM is uniform. In taking such a uniform electron density distribution, we also exclude the incoherent reflection of single electron or low-density electrons. Then, after some derivation we obtain the electric field amplitudes from equation (6) as

$$E'_{\rm r0} = E'_{\rm i0}(\omega_{\rm p}^2/2\gamma\omega_{\rm i}'^2)\sin(k'_{\rm i}l'), \tag{7}$$

where l' is thickness of the REM and $\omega_{\rm p} = (4\pi n_{\rm e}e^2/m_{\rm e})^{1/2}$ is the plasma frequency. Transforming back to the lab frame by $E_{\rm r0} = E'_{\rm r0}\gamma_z(1+\beta_z)$, $k'_{\rm i} = k_{\rm i}\gamma_z(1+\beta_z)$ and $l' = \gamma_z l$, the electric field amplitude of the reflected pulse will be intensified as

$$E_{\rm r0} = E_{\rm i0}\frac{\omega_{\rm p}^2}{2\gamma\omega_{\rm i}^2}\sin(k_{\rm i}l\gamma_z^2(1+\beta_z)) \sim \frac{1}{2\gamma}\frac{n_{\rm e}}{n_{\rm c}}E_{\rm i}. \tag{8}$$

The reflectivity is $\alpha = E_{\rm r0}^2\tau_{\rm r}/E_{\rm i0}^2\tau_{\rm i} \sim (1/4\gamma_z^2)(n_{\rm e}/2\gamma n_{\rm c})^2$.

Thus, the frequency upshift of the reflected pulse depends on the effective γ_z of the REM whereas the field amplitude intensification scales as the REM electron density in its moving frame $n_{\rm e}/\gamma$. Note that the scaling here is different from the incoherent reflection (scattering) from single electron or low-density electron beams [11], where the frequency upshift scales as $4\gamma^2$ ($\gamma_z \ll \gamma$).

3. 2D PIC simulations

3.1. Multidimensional demonstration of the scheme

To clearly demonstrate this novel scheme for laser frequency upshift and amplitude intensification, we perform 2D PIC simulations with the code `ILLUMINATION`. In the simulations, 25 000 cells along the laser axis z and 3000 cells transversely constitute a 12.5 μm $\times$ 30 μm box. Each cell is filled with 100 quasi-particles. The boundary conditions are absorbing for both electromagnetic waves and quasi-particles. We choose the same parameters as the above 1D simulation. A linearly x-polarized laser pulse at intensity $I_0 = 5 \times 10^{21}$ W cm^{-2} ($a_0 = 60$) and wavelength $\lambda = 1$ μm irradiates the foil at $t = 8.4T$ ($T \approx 3.3$ fs). The foil with density $n_0 = 200n_{\rm c}$ and thickness $l_0 = 5$ nm is assumed to be fully ionized as $m_{\rm i}/m_{\rm e} = 1836$ and initially locate at $z_0 = 4$ μm. The pulse is both temporally and transversely super-Gaussian of fourth order, $I \sim I_0\exp(-(r/r_0)^4)\exp(-[(t-t_0)/\tau]^4)$, where $r_0 = 8$ μm, $t_0 = 6T$ and $\tau = 21T$ are taken. This shape allows quasi-1D dynamics to be maintained and ensures the laser pulse

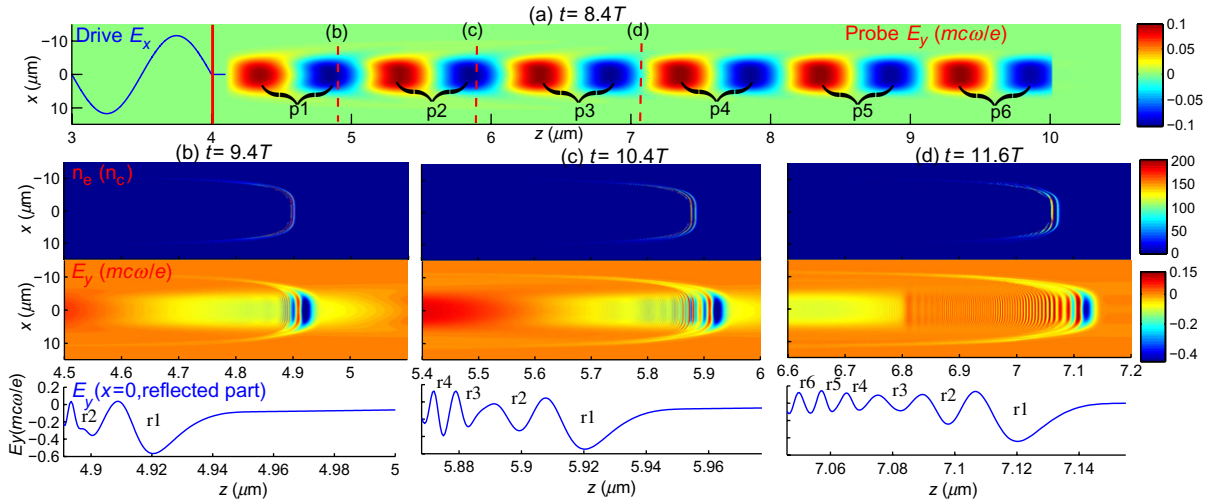

Figure 3. 2D PIC simulation for demonstration of the whole scheme (for parameters see text). (a) Electric field of the six-cycle counter-propagating probe pulse E_y at $t = 8.4T$, labeled 'p1'–'p6'. The blue solid line shows that the drive laser field E_x hits the foil (red solid line) at $t = 8.4T$, the dashed red lines show the positions that the blown-out electron sheet reaches at the time corresponding to (b)–(d). (b)–(d) Electron density n_e/n_c and E_y (including the transmitted and reflected parts) at, respectively, $t = 9.4$, 10.4 and $11.6T$. Between each time interval two cycles of the probe pulse are reflected. $E_y(x = 0$, reflected part) are the longitudinal profiles for the reflected part of E_y before the rear/leftmost side of the sheet (also six cycles labeled 'r1'–'r6'). The results are also presented in detail in movie 1 (stacks.iop.org/NJP/11/103042/mmedia).

with very sharp front. A weak probe pulse with $I_i = 1.37 \times 10^{16}\,\mathrm{W\,cm^{-2}}$ ($a_i = 0.1$) and $\lambda_i = 1\,\mu$m propagates antiparallelly from the right boundary at $t = 0$. The probe pulse has similar shape, $I \sim I_i \exp(-(r/r_i)^4)\exp(-[(t - t_i)/\tau_i]^4)$, where $r_i = 5\,\mu$m ensuring that the reflection is from the central plane part of the REM, $t_i = 3T$ and $\tau_i = 10T$ (i.e. the pulse has only six cycles). The electric field of the probe pulse is y-polarized orthogonal to that of the drive pulse so that their fields can be clearly separated in the simulation.

Figures 3(b)–(d) show electron density n_e/n_c, electric field of the incident probe, transmitted and reflected pulses E_y at $t = 9.4$, 10.4 and $11.6T$. The evolutions of these quantities as well as the drive laser electric field E_x from $t = 8.0T$ for the whole physical process are presented in detail in movie 1 (stacks.iop.org/NJP/11/103042/mmedia). In accordance with the previous 1D simulation and the theoretical expectation, all electrons in the laser focal spot ($x < 8\,\mu$m) are blown out, forming a dense electron sheet with density above $200n_c$, thickness about 10 nm and $\gamma_z \approx 4.5$ (shown in figure 5(a)) at $t = 9.4T$. The electron sheet becomes relativistic quickly, so the transverse instabilities [16, 17] (such as Rayleigh–Taylor-like or Weibel-like) are also much suppressed as their growth becomes γ times slower in the moving frame due to the relativistic effect. The electron sheet decompresses slowly with time due to E_z. The z-axis coordinates of electrons at the leftmost and rightmost sides of the sheet varying with t are plotted in figure 2(b), also conforming to the solution from the theoretical model

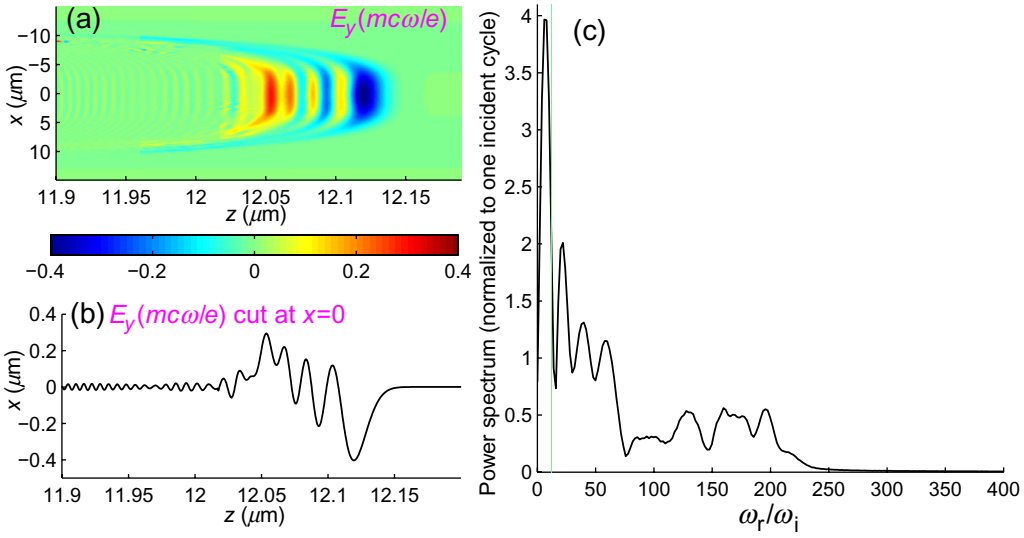

Figure 4. (a) The pure reflected pulse E_y at $t = 16.6T$ in the simulation of figure 3 when it has completely separated from the transmitted pulse; (b) its longitudinal profile cut at $x = 0$; (c) the corresponding power spectrum, which shows several peaks due to the reflections at different mean γ_z of the REM during its acceleration, and sharp cut-off at $\omega_r/\omega_i \approx 220$ in good agreement with that expected from the last reflection at $\gamma_z \approx 7.3$, shown in figure 5(c). The y-axis amplitude of the spectrum is normalized to that of one cycle incident probe pulse, which therefore represents the intensification for the reflected field too.

(equations (2)–(4)) with the initial time $t_0 = 8.4T$ and position $z_0 = 4.0\,\mu$m. Up to $t = 11.6T$ the electron sheet still has a thickness of only 20 nm, with density above $100n_c$ and mean $\gamma_z \approx 7.3$ (see 5(c)). The flying electron sheet can therefore be taken as a near-ideal REM during this time interval.

The counter-propagating probe pulse (shown by E_y in figure 3) hits this flying REM at about $t = 8.47T$ a little later than the drive pulse hits the foil. Since the relative velocity between the REM and the probe pulse is about twice the speed of light, two cycles of the probe pulse have been reflected in each of the time intervals at about one laser cycle T (between figures 3(a)–(d), for details see movie 1). The reflected pulse (label 'r1'–'r6') has the same number of cycles as the incident probe pulse ('p1'–'p6'), since this is Lorentz invariant. The respective wavelengths of six cycles for the reflected pulse λ_r decrease from about 48 to 5 nm, i.e. from 21 to 200 times less than the incident λ_i. This is because the reflections of each cycle occur at different γ_z during the REM acceleration. This also verifies the theoretical expectation (5), for examples, $\lambda_r \approx 13$, 8.5 and 5 nm of 'r2', 'r4', 'r6' approximately corresponds to mean $\gamma_z = 4.5$, 5.8 and 7.3 in figures 5(a)–(c). The reflected pulse is along the normal direction of the REM, further confirming coherent scattering. For incoherent scattering, reflection is along the electron velocity direction. After $t = 11.6T$ the whole probe pulse has already interacted with the REM, the transmitted part propagates to the left boundary and the reflected part to the right boundary, both are completely separated.

Figures 4(a) and (b) describe the pure reflected radiation pulse at $t = 16.6\,T$. The reflected pulse is strongly chirped due to the acceleration of the REM and is also heavily compressed

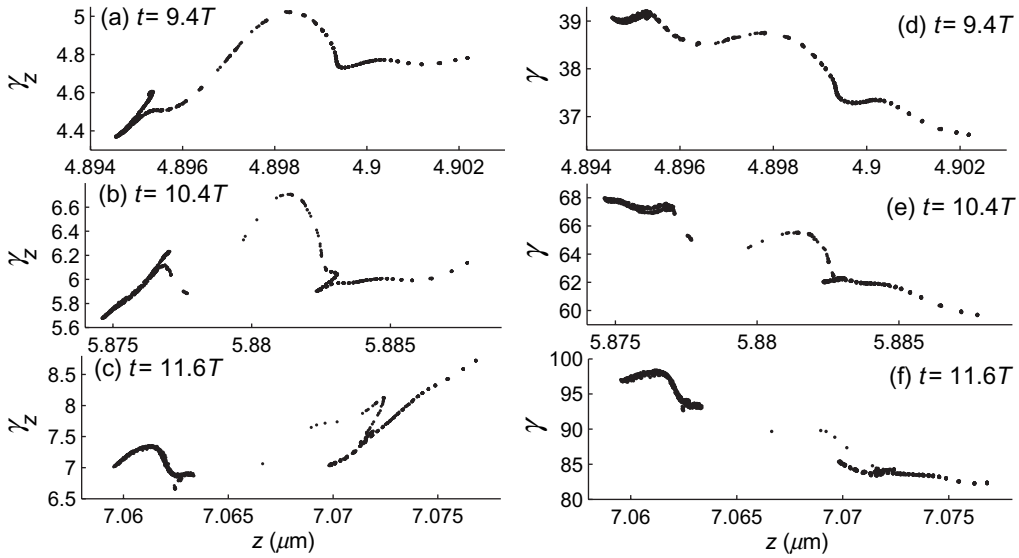

Figure 5. (a)–(c) The sheet electron phase spaces (for electrons near the axis within $-2.5\,\mu\text{m} < x < 2.5\,\mu\text{m}$) of the effective Lorentz factor along the normal direction of the REM $z - \gamma_z$ at $t = 9.4, 10.4, 11.6T$ in the simulation of figure 3, which verify that the frequency upshift conforms to the theoretical expectation (5). (d)–(f) are the corresponding full Lorentz factors $z - \gamma$, which have relation to the amplitude intensification as equation (8).

(pulse duration about 430 attosecond) due to the frequency upshift. The corresponding power spectrum in figure 4(c) shows several peaks due to the reflections occurring at different mean γ_z of the REM during its acceleration, such as those given in figures 5(a)–(c) at different time. The sharp cut-off frequency of the reflected pulse is $\omega_r/\omega_i \approx 220$. This is in excellent agreement with the expectations for $\gamma_z \approx 7.3$ (see figure 5(c)), implying a relativistic Doppler shift (equation (5)) $\omega_r/\omega_i \approx 4\gamma_z^2 \approx 213$. Furthermore, the amplitude of the reflected field decreases from $E_r \approx 4.0E_i$ to $0.5E_i$, as shown in figure 4(b) or (c). This also agrees well with equation (8) as $E_r/E_i \approx (1/2\gamma)(n_e/n_c)$, because the mean γ of the REM increases from about 24–98 (see figure 5(f) for $t = 11.6T$) while the average density decreases from $200n_c$ to $100n_c$ during the acceleration. The average (integrated) reflectivity of the REM for the whole six-cycle probe pulse α is about 20%.

3.2. Additional simulation results with different parameters

As analyzed in section 2, the scheme can also be fulfilled for lower intensity lasers (a_0) using a lower mass density ($\sigma_0 = n_0 l_0$) foil. For example, we choose the foil with a lower density of $n_0 = 100n_c$ and thickness $l_0 = 5\,\text{nm}$, and decrease the drive laser intensity to $I_0 = 2 \times 10^{20}\,\text{W cm}^{-2}$ ($a_0 = 12$), which is within reach of current laser systems in laboratories. The same probe pulse is chosen. The simulation results are presented in detail in movie 2 (stacks.iop.org/NJP/11/103042/mmedia), describing the evolutions of n_e/n_c, E_x and E_y from $t = 8.0T$. Figure 6 shows the pure reflected pulse E_y at $t = 16.6T$ ((a) and (b)) and its corresponding power spectrum (c). We see that the reflected pulse is also strongly chirped and heavily compressed, similarly to the above case. Its frequency is Doppler upshifted and the cut-off frequency in the spectrum (c) is $\omega_r/\omega_i \approx 95$, which also conforms well to that expected from

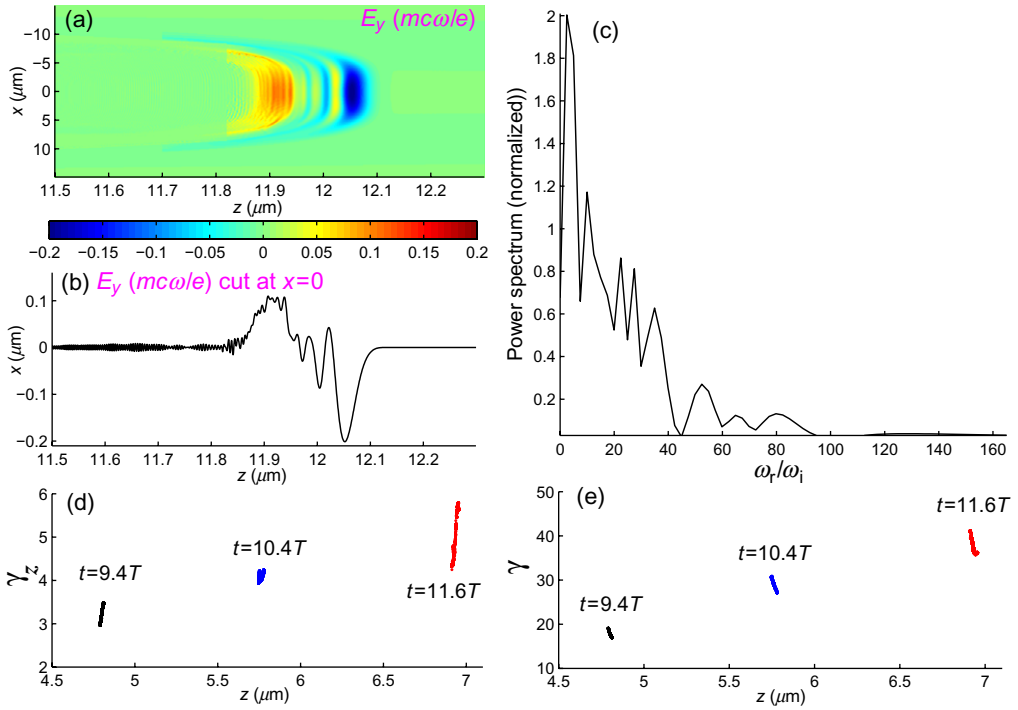

Figure 6. 2D simulation results by choosing a lower density foil as $n_0 = 100n_c$ and decreasing the drive laser intensity as $a_0 = 12$ (other parameters are the same as figure 3): (a) The pure reflected pulse E_y at $t = 16.6T$; (b) its longitudinal profile cut at $x = 0$; (c) the corresponding power spectrum, conforming well to the theoretical expectations; (d) and (e) electron phase space $z - \gamma_z$ and $z - \gamma$ at $t = 9.4$, 10.4, $11.6T$ for the electrons of the sheet near the axis within $-2.5\,\mu\text{m} < x < 2.5\,\mu\text{m}$. The results are also presented in detail in movie 2 (stacks.iop.org/NJP/11/103042/mmedia).

the theoretical analysis (equation (5)) as mean $\gamma_z \approx 5$ (see figure 6(d)) and $4\gamma_z^2 \approx 100$. However, the amplitude of the reflected pulse decreases rapidly from $E_r \approx 2.0E_i$ to $0.18E_i$, because the density of the REM decreases from $100n_c$ to only $20n_c$ while the full γ increases from about 20–45 (see figure 6(e)), in accordance with equation (8) as well. The average (integrated) reflectivity of the REM α decreases to about 8%.

4. Conclusion and discussion

In conclusion, we have self-consistently shown that coherent x-ray sources can be obtained by reflection of a counter-propagating probe pulse from dense electron sheets blown-out from laser-irradiated ultrathin foils, applying theoretical modeling and 2D PIC simulations. An analytical RPA model for the dynamics of the electron sheet is presented and verified by PIC simulations. Such electron sheet is a transient coherent structure with its lifetime depending critically on the laser amplitude a_0 and the foil areal density $\sigma_0 = n_0 l_0$. A quantitative analysis for the reflected pulse from the sheet is integrally given afterwards. It is found that the reflected pulse undergoes frequency upshift by a factor $4\gamma_z^2$, where $\gamma_z = (1 - v_z^2/c^2)^{-1/2}$ is the effective Lorentz factor

of the mirror along its normal direction, and amplitude intensification by a factor scaling as the mirror electron density in its moving frame n_e/γ, where γ is the full Lorentz factor. The 2D PIC simulations have, for the first time, integrally and quantitatively demonstrated this novel scheme for coherent x-ray source production, in agreement with the theory. The reflected pulse sources here are very different from the incoherent pulse scattering from single electron (or low-density electron beams) [11], where the photon frequency is upshifted by the factor $4\gamma^2$.

Note that linearly polarized lasers are chosen in the simulations in order to clearly separate the fields of the drive and probe pulses in the simulation. For circularly polarized lasers, the ponderomotive force is steady [19] and dense electron sheet may possibly be stable for a longer time duration, which is favorable for use as relativistic mirrors. Here, the reflected pulse is chirped and the reflectivity of the mirror decreases with time due to the mirror acceleration. Choosing a sufficiently high-density foil and a ultrashort probe pulse sent with an appropriate delay, one can obtain a single nanosecond x-ray pulse at keV photon energy.

Acknowledgments

The work was supported by EPSRC (grants EP/C003586/1 and EP/D/06337X/1). MZ acknowledges the support from the Royal Society. BQ acknowledges the support from the Alexander von Humboldt Foundation and useful discussions with X T He and C T Zhou at Center for Applied Physics and Technology, Peking University.

References

[1] Maiman T H 1960 *Nature* **187** 493
[2] Daido H 2002 *Rep. Prog. Phys.* **65** 1513
[3] Ackermann W *et al* 2007 *Nat. Photonics* **1** 336
[4] Zepf M *et al* 2007 *Phys. Rev. Lett.* **99** 143901
[5] Schwoerer H *et al* 2006 *Phys. Rev. Lett.* **96** 014802
[6] Bulanov S V *et al* 2003 *Phys. Rev. Lett.* **91** 085001
[7] Kando M *et al* 2007 *Phys. Rev. Lett.* **99** 135001
[8] Dromey B *et al* 2006 *Nat. Phys.* **2** 456
[9] Dromey B *et al* 2007 *Phys. Rev. Lett.* **99** 085001
[10] Kulagin V V *et al* 2007 *Phys. Rev. Lett.* **99** 124801
Kulagin V V *et al* 2007 *Phys. Plasmas* **14** 113101
[11] Habs D *et al* 2008 *Appl. Phys.* B **93** 349
[12] Meyer-ter-Vehn J and Wu H-C 2009 *Eur. Phys. J.* D DOI: 10.1140/epjd/e2009-00081-1
Wu H-C and Meyer-ter-Vehn J 2009 *Eur. Phys. J.* D DOI: 10.1140/epjd/e2009-00082-0
Wen M *et al* 2009 *Eur. Phys. J.* D DOI: 10.1140/epjd/e2009-00083-y
[13] Esirkepov T *et al* 2004 *Phys. Rev. Lett.* **92** 175003
[14] Yan X Q *et al* 2008 *Phys. Rev. Lett.* **100** 135003
[15] Qiao B *et al* 2009 *Phys. Rev. Lett.* **102** 145002
[16] Pegoraro F and Bulanov S V 2007 *Phys. Rev. Lett.* **99** 065002
[17] Yan X Q *et al* 2009 *Phys. Plasmas* **16** 044501
[18] Esirkepov T *et al* 2009 *Eur. Phys. J.* D (at press)
[19] Macchi A *et al* 2005 *Phys. Rev. Lett.* **94** 165003